Journal of Experimental Botany Advance Access published February 22, 2010

Journal of Experimental Botany, Page 1 of 17
doi:10.1093/jxb/erq018

Journal of Experimental Botany
www.jxb.oxfordjournals.org

RESEARCH PAPER

Development and verification of a water and sugar transport model using measured stem diameter variations

Veerle De Schepper* and Kathy Steppe

Laboratory of Plant Ecology, Department of Applied Ecology and Environmental Biology, Faculty of Bioscience Engineering, Ghent University, Coupure links 653, B-9000 Ghent, Belgium

* To whom correspondence should be addressed. E-mail: Veerle.DeSchepper@UGent.be

Received 4 August 2009; Revised 14 January 2010; Accepted 21 January 2010

Abstract

In trees, water and sugars are transported by xylem and phloem conduits which are hydraulically linked. A simultaneous study of both flows is interesting, since they concurrently influence important processes such as stomatal regulation and growth. A few mathematical models have already been developed to investigate the influence of both hydraulically coupled flows. However, none of these models has so far been tested using real measured field data. In the present study, a comprehensive whole-tree model is developed that enables simulation of the stem diameter variations driven by both the water and sugar transport. Stem diameter variations are calculated as volume changes of both the xylem and the phloem tissue. These volume changes are dependent on: (i) water transport according to the cohesion–tension theory; (ii) sugar transport according to the Münch hypothesis; (iii) loading and unloading of sugars; and (iv) irreversible turgor-driven growth. The model considers three main compartments (crown, stem, and roots) and is verified by comparison with actual measured stem diameter variations and xylem sap flow rates. These measurements were performed on a young oak (*Quercus robur* L.) tree in controlled conditions and on an adult beech (*Fagus sylvatica* L.) tree in a natural forest. A good agreement was found between simulated and measured data. Hence, the model seemed to be a realistic representation of the processes observed in reality. Furthermore, the model is able to simulate several physiological variables which are relatively difficult to measure: phloem turgor, phloem osmotic pressure, and Münch's counterflow. Simulation of these variables revealed daily dynamics in their behaviour which were mainly induced by transpiration. Some of these dynamics are experimentally confirmed in the literature, while others are not.

Key words: Diurnal cycles, *Fagus sylvatica* L., growth, modelling, Münch hypothesis, phloem translocation, *Quercus robur* L., sap flow, stem diameter variations, xylem.

Introduction

In trees, efficient water and sugar transport systems are essential to sustain growth and development. Water and sugars are transported by xylem vessels and phloem tubes, respectively. Since these two conduits are hydraulically connected, it can be expected that both transport processes are physiologically coupled. A thorough understanding of this coupling can be of importance because water and sugar transport concurrently influence plant processes such as stomatal conductance and growth. Recently, attempts have been made to model the hydraulic linkage between xylem vessels and phloem tubes mechanistically (Daudet *et al.*, 2002; Hölttä *et al.*, 2006; Lacointe and Minchin, 2008). These models include the basic concepts of water and carbon transport.

Water transport in these models is commonly driven by transpiration, which sets up a water potential gradient between the soil and the leaves so that water flows (Jones, 1992). This water flow is often mathematically described by the concept of 'van den Honert' (1948) and presents a simple Ohm's law analogy. However, in order to be able to describe the actual time lag between transpiration and water uptake from the soil, van den Honert's concept needs to be

extended by taking into account internal water reserves in the plant (Steppe *et al.*, 2006*a*). Sugar transport, the other key process in these models, is often described by the well-known Münch theory (Münch, 1930). According to this theory, the flow phenomenon occurring in the phloem is induced by a gradient in turgor pressure which, in turn, is caused by a difference in sugar concentration between the regions of phloem loading and unloading (Münch, 1930). The preservation of this gradient depends on the balance between the loading processes at the sources (typically leaves) and the unloading processes at the sinks (e.g. roots and fruits) (Ortega *et al.*, 1988; Gamalei, 2002). Furthermore, a radial water flow, existing between the xylem vessels and the phloem tubes, is proportional to a difference in water potential (Daudet *et al.*, 2002; Hölttä *et al.*, 2006; Lacointe and Minchin, 2008).

The few existing models in the literature (Daudet *et al.*, 2002; Hölttä *et al.*, 2006; Lacointe and Minchin, 2008) show that the proposed mechanisms briefly summarized above are quantitatively plausible. However, none of these models was tested using real measured field data. Therefore, a comprehensive whole-tree model was developed, describing the hydraulic link between water and sugar transport. The presented model incorporates the main concepts of the leading transport models in the literature (Daudet *et al.*, 2002; Hölttä *et al.*, 2006; Lacointe and Minchin, 2008) together with irreversible radial stem growth (Table 1). The main objective of the present study was to test this model using actual data collected in both controlled and forest conditions. To this end, a model output needed to be selected which was measurable and was simultaneously influenced by water and carbon transport. Since stem diameter variations can easily be measured on wooden trees and since they are influenced by both the carbon and the water status in the tree (Daudet *et al.*, 2005), they were selected as appropriate measurements with which the model output could be compared. Other carbon-related variables are known to be more difficult to measure on a whole-tree level (Gould *et al.*, 2004; Windt *et al.*, 2006).

Table 1. The difference between recent models in the literature describing simultaneously water and sugar transport in plants

	Model of Daudet *et al.* (2002)	**Model of Höllta *et al.* (2006)**	**Model of Lacointe *et al.* (2008)**	**Model described in this study**
Model structure detail level				
Plant parts: vertical compartments (no. of discrete vertical elements)	Roots (1) Stem (8) Leaves (3) Fruits (3)	Stem (40)	Shoots (3) Stem (9) Roots (6)	Roots (1) Stem (1) Leaves (1)
Stem tissues: radial compartments	Xylem tissue	Non-functional xylem (heartwood)	Xylem tissue	Non-functional xylem
	Phloem tissue	Functional xylem (sapwood) Cambium Functional phloem Non-functional living cells	Phloem tissue	Functional xylem Cambium Functional phloem Non-functional living cells
Architectural complexity	Mediated	Low	High	Low
Data	Theoretical	Theoretical	Theoretical	Obtained by experiments
Model dimension	One dimension (time)	One dimension (time)	One dimension (time)	One dimension (time)
Processes				
Axial water flow	According to pressure gradient	According to pressure gradient	According to pressure gradient	According to pressure gradient
Radial water flow	According to water potential gradient	According to water potential gradient	According to water potential gradient	According to water potential gradient
Axial sugar flow	According to mass transport	According to mass transport	According to mass transport	According to mass transport
Loading rate	Function of starch concentration in leaf	Constant	Constant or function of sugar concentration in leaf	Function of sugar concentration in leaf
Unloading rate	–	Function of sugar concentration in phloem	Constant or function of sugar concentration in phloem	Function of sugar concentration in phloem
Reversible swelling of stem	No	Yes	No	Yes
Irreversible stem growth	No	No	No	Yes
Starch metabolism	Yes	No	Yes	Yes
Respiration	Yes	No	Yes	Yes
Sensitivity analysis	Manual	Manual	No	Computational

In stem diameter variations two important components can be distinguished. The first component is the reversible stem diameter fluctuation, which results from a time lag between leaf transpiration and root water uptake (Steppe and Lemeur, 2004). This time lag causes internal water reserves in the stem to be depleted and refilled on a daily basis, which causes the stem to shrink in the morning and to swell in the evening (Génard *et al.*, 2001; Perämäki *et al.*, 2005; Steppe *et al.*, 2006*a*). Hence, these reversible fluctuations mainly depend on the water content of the internal stem water reserves (Zweifel *et al.*, 2001; Goldhamer and Fereres, 2004; Steppe *et al.*, 2006*a*). The second component represents radial stem growth and is irreversible. It will only appear when sufficient water and sugars are available. First, a sufficiently high water content is necessary for the build-up of turgor (i.e. positive pressure) in the stem cells (Lockhart, 1965; Proseus *et al.*, 1999). Secondly, sugars are required for their incorporation in cell walls when structural expansion appears (Zweifel *et al.*, 2006) and for sustaining the maintenance respiration of the living stem cells (Teskey *et al.*, 2008). As a result, stem diameter variations are influenced by both the water and carbon transport, making it a valuable variable for testing the model.

Materials and methods

Plant material

In order to be able to test the model, two trees of a different genus and age, and growing in a different environment were selected. The first tree (T1) was a 3-year-old oak tree (*Quercus robur* L.) growing in a 50.0 l container in a growth chamber at the Laboratory of Plant Ecology of Ghent University (Belgium) with dimensions 2×1.5×2 m (height×width×length). At the beginning of the experiment, the tree was 1.6 m high and had a stem diameter of 21.4 mm at the soil surface. The growth chamber allowed the control of radiation and air temperature, while relative humidity of the air fluctuated freely depending on radiation, air temperature, and the transpiration rate of the trees. The tree was watered every 2–3 d to ensure the potting mixture remained adequately watered. The second tree (T2) was an 89-year-old beech tree (*Fagus sylvatica* L.) growing in the mixed deciduous experimental forest Aelmoeseneie, located in Gontrode, Belgium (50°58′N, 3°49′E). The tree was 27 m high and had a diameter at breast height of 57 cm. Ecophysiological measurements at different heights in the crown were possible due to the presence of a 35 m high measuring tower next to the beech tree. The measurements took place from 19 to 23 August 2008 [day of year (DOY) 231–235] in the growth chamber and in the forest from 17 to 22 August 2008 (DOY 229–234).

Meteorological measurements

A few meterorological variables were continuously measured at both sites. Quantum sensors (Li-190S, Li-COR, Lincoln, NE, USA) were used to measure photosynthetic active radiation (PAR) and were installed at a height of 1.7 m and 26 m above the soil surface for T1 and T2, respectively. Soil water potential (ψ_{soil}) was measured with an electronic tensiometer [SWT6 (T1) and SWT4 (T2), Delta-T, Cambridge, UK] and air temperature (T) with a copper–constantan thermocouple (Omega, Amstelveen, The Netherlands) which was installed at the same height as the PAR sensor.

Physiological measurements

Continuous measurements of leaf net photosynthesis (P_n) and transpiration (E) were used as model inputs, while stem diameter variation measurements were used for testing and calibrating the model. P_n was measured with branch cuvettes connected to an infrared gas analyser [IRGA-225-MK3 CO_2, ADC, Hertfordshire, UK (T1); ADC 2250 Gas Analyser, ADC BioScientific Ltd, UK (T2)]. A branch cuvette of low density polyethylene was installed at ~1.5 m height on T1 and enclosed a leaf area of 66 cm^2. The branch cuvette of T2 was constructed of teflon–perfluoralkoxy. It was installed at ~21 m height and enclosed a leaf area of ~530 cm^2. Air from outside was blown into the branch cuvettes at a rate of 4 l min^{-1}. A gas multiplex system was used to sample the cuvettes during sampling periods of 10 min and 15 min for T1 and T2, respectively. During each sampling period, the incoming and outgoing air of the cuvette was continuously monitored, but only the stable readings of the last 3 min were averaged and used for calculations. After each sampling period, a zero measurement was carried out to detect possible drifts in the zero point reading of the IRGA.

Transpiration (E) and xylem stem sap flow (F^X_{stem}) of T1 were measured with sap flow sensors based on the heat balance (HB) principle (SGA5 and SGA10, Dynamax Inc., Houston, TX, USA). The SGA5 sensor was installed on a first-order branch and was used to estimate E, while the SGA10 sensor was installed on the main stem and used to estimate F^X_{stem}. These sensors were thermally insulated with several layers of aluminium foil wrapped around the sensors. E and F^X_{stem} were calculated according to the approach of Steppe *et al.* (2005) to eliminate errors induced by heat storage effects. Sheath conductance of the gauge was recalculated daily using minimum values observed during the dark period between 00:00 h and 06:00 h. The value of 0.42 W m^{-1} $°C^{-1}$ for thermal conductance of woody stems was taken from Steinberg *et al.* (1989). E and F^X_{stem} of T2 were measured with thermal dissipation probes (TDP-30, Dynamax Inc., Houston, TX, USA) (Granier 1985, 1987) installed in the stem at 14 m and 1.5 m height, respectively.

Variations in stem diameter were continuously measured with linear variable displacement transducers (LVDTs) [model DF5.0, Solartron Metrology, Leicester, UK (T1); model LP-20F-6, Natkon, Hombrechtikon, Switzerland (T2)]. One LVDT was installed on the stem bark at a height of 30 cm and 14 m for T1 and T2, respectively, to measure reversible and irreversible variations. On T2, a second LVDT sensor was installed ~10 cm below the first one with its contact tip placed on a screw screwed through the bark into the xylem. Hence, this sensor excluded growth and volume fluctuations of the bark (Sevanto *et al.*, 2003). A similar measurement was not possible for T1, since the stem diameter was too small to fix the screw well.

The leaf and stem water potential of T1 were measured offline with a pressure chamber (PMS Instruments, Corvallis, OR, USA) at DOY 233. Stem water potential was measured on leaves that were prevented from transpiration for a minimum of 1 h by enclosing the leaves in an aluminium envelope.

All signals from the online sensors were logged at 10 s intervals, and 5 min means were stored using either a data logger (in the growth chamber, T1, DL2, Solartron Metrology, Leicester, UK) or a data acquisition system (in the field, T2, type 34980A, Agilent, California, USA). Except for the IRGA measurements 1 min means were stored.

Model description

The main purpose of the model is to describe water and sugar transport through an entire living tree. In addition, the model is able to simulate stem diameter variations which result from both concurrent transport processes. As explained earlier, these stem diameter variations are an essential variable for model testing using the actual tree data. Furthermore, respiration and starch conversion are

included in the model to complete the carbon balance. Model design is based on the diagrams depicted in Fig. 1. Lists of all model variables and parameters (including units and definitions) are presented in Tables 2 and 3.

Model structure

The model tree is divided into three main compartments (j) in the vertical direction: the crown compartment representing the leaves and branches, the stem compartment representing the trunk, and the root compartment representing all the existing roots (Fig. 1). Each of these main compartments is divided into several radial subcompartments (i) representing different tissues. Both the crown and root compartment have three subcompartments: active xylem vessels (X), active phloem tubes (Pc), and storage cells which represent the local parenchyma cells (S). The stem compartment consists of five subcompartments: the non-conductive xylem vessels or heartwood (H), the conducting xylem vessels or sapwood (X), the cambial zone with cell division and cell differentiation (Cz), the conductive phloem (Pc), and the cortex with a storage function (S). Each subcompartment is separated from its radial adjacent subcompartment by a semi-permeable membrane. These virtual membranes represent all cell membranes which water and solutes have to pass to flow from one tissue (subcompartment) to another (Génard *et al.*, 2001; Steppe *et al.*, 2006*a*). Therefore, the stem tissues are modelled as five coaxial cylinders radially separated from each other by virtual membranes (Fig. 1). The adjacent vertical compartments (X and Pc) are not separated by membranes, because real xylem vessels and phloem tubes contain perforation plates and sieve plates, respectively.

Concept of dynamic water transport

Transpiration is used as input for the water transport submodel. The soil is considered as a non-limiting external

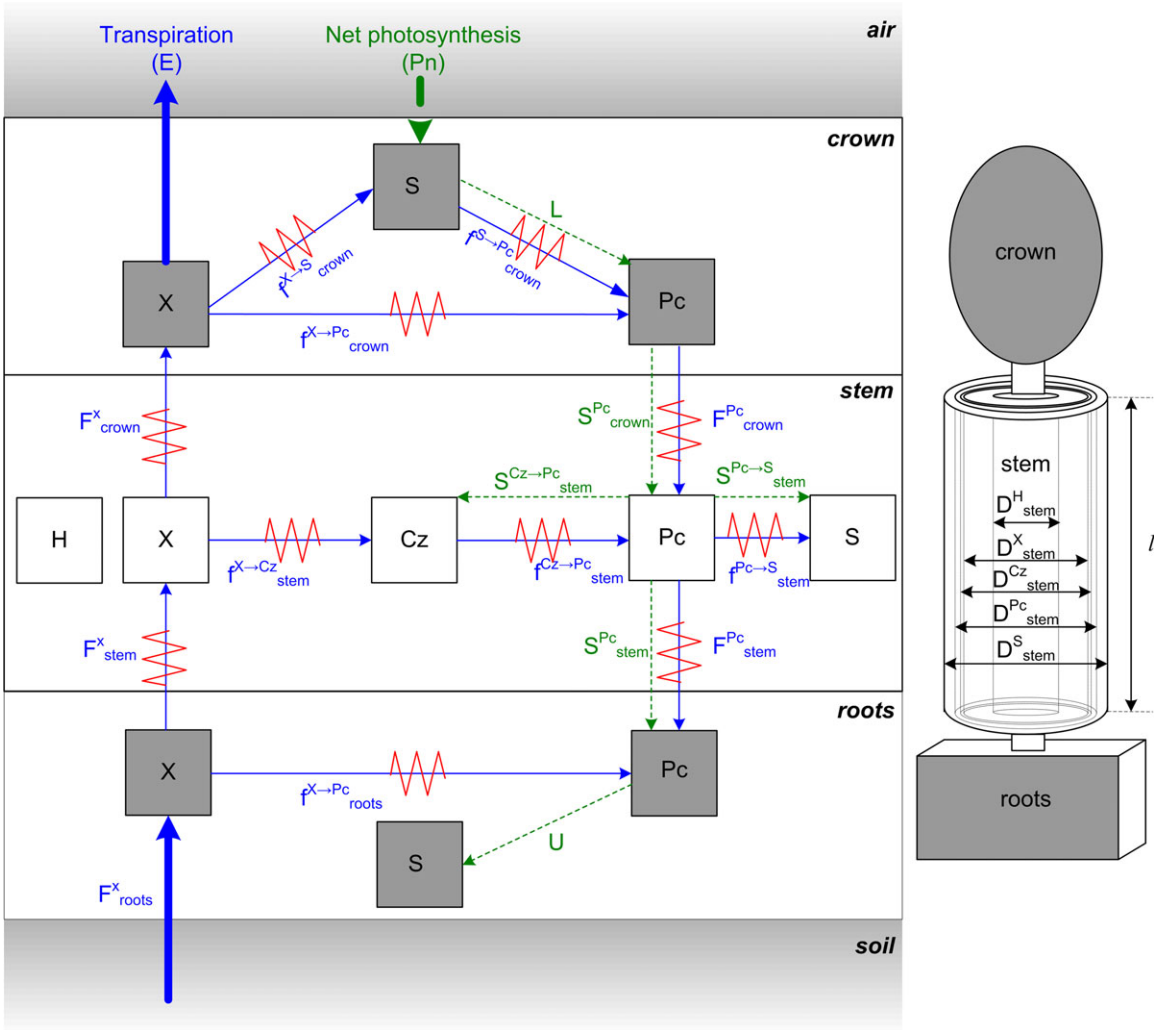

Fig. 1. Model schematic with model compartments (X, conductive xylem; Pc, conductive phloem; S, storage cells; Cz, cambial zone) and water (full line) and sugar (dotted line) transport. This transport can occur in both directions: the flow is considered positive when it is in the direction of the arrow and negative when it is in the opposite direction. The resistances between two adjacent cells are also indicated. The stem consists of five coaxial cylinders with length *l* and with diameter D. Each cylinder represents a stem tissue: heartwood (H), conductive xylem (X), cambial zone (Cz), and conductive phloem (Pc), and storage cell, e.g. cortex (S). D^{S}_{stem} is equal to the total stem diameter. The coaxial cylinders are separated from each other by virtual membranes.

Table 2. Symbol, unit, and description of the model variables

Symbol	Unit	Description
F_j^i	[mg s^{-1}]	The vertical water flow in the xylem (i=X) and phloem (i=Pc)
$f_j^{i\to i+1}$	[mg s^{-1}]	The radial water flow rate between two radial adjacent compartments
P_j^i	[MPa]	Turgor pressure or tension
$\prod_j^i$	[MPa]	Osmotic pressure
$R_j^{i\to i+1}$	[MPa s mg^{-1}]	The radial resistance between two radial adjacent compartments
$A_{rad}^{i\to i+1}$	[m^2]	The radial surface interface between the stem compartments
T	[°C]	The air temperature
C_j^i	[mg m^{-3}]	The sucrose concentration
W_j^i	[mg]	The mass of water
S_j^{Pc}	[mg sucrose s^{-1}]	The sucrose transport rate in phloem tubes
L	[mg sucrose s^{-1}]	The loading rate in the crown
U	[mg sucrose s^{-1}]	The unloading rate in the roots
$s_{stem}^{i\to i+1}$	[mg sucrose s^{-1}]	The exchange rate of sucrose between radial adjacent compartments in the stem
ϵ_j^i	[MPa]	The bulk elastic modulus
V_j^i	[m^3]	The volume of the compartment
f_{stem}^{Cz}	[v/v]	The fraction of water in the cambial stem zone
D_{stem}^i	[m]	Diameter of the coaxial cylinder representing the compartment
St_j^S	[mg]	The mass of starch
C_0	[mg sucrose m^{-3}]	The target sucrose concentration in the storage tissues
Rm_j^S	[mg sucrose s^{-1}]	The maintenance respiration of the storage tissues
Rg_{stem}^{Cz}	[mg sucrose s^{-1}]	The growth respiration of the cambial zone

Table 3. Symbol, unit, and description of the model parameters

Symbol	Unit	Description
σ	[dimensionless]	The reflection coefficient between two radial adjacent compartments
ρ_w	[mg m^{-3}]	The density of water
ρ_{wood}	[mg m^{-3}]	The density of dry wood
R^X	[MPa s mg^{-1}]	The vertical resistance in the xylem vessels
R^{Pc}	[MPa s mg^{-1}]	The vertical resistance in the phloem tubes
$R_{roots}^{X\to Pc}$	[MPa s mg^{-1}]	The radial resistance in the roots
$R_{crown}^{X\to Pc}$	[MPa s mg^{-1}]	The radial resistance in the crown
L_{rad}	[m MPa^{-1} s^{-1}]	The radial hydraulic conductivity
$MM_{sucrose}$	[mg mol^{-1}]	The molar mass of sucrose
R	[MJ mol^{-1} K^{-1}]	The universal gas constant
$V_{max,L}$	[mg sucrose s^{-1}]	A kinetic parameter of the loading rate
$K_{M,L}$	[mg m^{-3}]	A kinetic parameter of the loading rate
k_U	[mg s^{-1}]	The unloading rate when sucrose concentration in the phloem tubes and the storage tissue is equal
$k_{lat}^{Cz\to S}$	[m^3 s^{-1}]	The kinetic constant for lateral sucrose diffusion
$k_{lat}^{Pc\to S}$	[m^3 s^{-1}]	The kinetic constant for lateral sucrose diffusion
ϵ_∞^S	[MPa]	The maximum bulk elastic modulus when P is large for the storage tissues
ϵ_∞^{Pc}	[MPa]	The maximum bulk elastic modulus when P is large for the phloem tubes
ϵ^X	[MPa]	The xylem bulk elastic modulus
φ	[MPa^{-1} s^{-1}]	The cell wall extensibility
Γ	[MPa]	The threshold turgor
l	[m]	The length of the stem
k_{starch}	[m^3 s^{-1}]	A kinetic parameter for starch conversion
$k_{Rm,1}$	[mg sucrose m^{-3} s^{-1}]	A kinetic parameter for maintenance respiration
$k_{Rm,2}$	[s^{-1}]	A kinetic parameter for maintenance respiration
Y	[dimensionless]	The growth efficiency or yield

water pool with a constant water potential. All compartments in the model contain a certain amount of water and are hydraulically linked to each other (full arrows in Fig. 1). Transpiration starts a chain of water flows throughout the entire tree. These vertical and radial water flows are mathematically described by van den Honert (1948) and Kedem and Katchalsky (1958), respectively (units of the variables are placed between square brackets):

$$\text{vertical flow}: F_j^i = \frac{P_j^i - P_{j+1}^i}{R_j^i} \quad (1)$$

$$\text{radial flow}: f_j^{i\to i+1} = \frac{\left(P_j^i - P_j^{i+1}\right) - \sigma\left(\prod_j^i - \prod_j^{i+1}\right)}{R_j^{i\to i+1}} \quad (2)$$

with F_j^i the vertical sap flow rate [mg s^{-1}], $f_j^{i\to i+1}$ the radial sap flow rate [mg s^{-1}], P_j^i the turgor in living cells or the tension (i.e. negative pressure) in the xylem vessels [MPa], $\prod_j^i$ the osmotic pressure in the living cells [MPa], $R_j^{i\to i+1}$ the resistance between two adjacent compartments [MPa s mg^{-1}], σ the reflection coefficient between two radial adjacent compartment [dimensionless], j the main compartment (roots, stem, and crown), and i the subcompartments (X, Cz, Pc, S). σ is set equal to 1, since it is assumed that no solutes can pass the semi-permeable membrane. When T2 is considered, a gradient in P of –0.01 MPa m^{-1} is considered to counteract the gravitational potential (Jones, 1992). The xylem water potential of the roots (P_{roots}^X) was set equal to the averaged measured soil water potential (ψ_{soil}) multiplied by a factor. This approximation is justified because the model aims at simulating physiological processes within the tree, and not between the soil and the tree (Steppe *et al.*, 2006*a*).

The axial flow resistances were assumed to be equal in the stem and the crown compartment ($R_{crown}^X = R_{stem}^X = R^X$ and $R_{crown}^{Pc} = R_{stem}^{Pc} = R^{Pc}$). Furthermore, all radial flow

resistances are equal in the crown compartment ($R_{crown}^{X\rightarrow Pc} = R_{crown}^{X\rightarrow S} = R_{crown}^{S\rightarrow Pc}$), while the radial flow resistances in the stem compartment are inversely proportional to the radial hydraulic conductivity (L_{rad} [m MPa^{-1} s^{-1}]):

$$R_{stem}^{i\rightarrow i+1} = \frac{1}{L_{rad} A_{rad}^{i\rightarrow i+1} \rho_w} \quad (3)$$

with ρ_w the density of water [mg m^{-3}] equal to 10^9 (Forsythe, 1954;2003) and $A_{rad}^{i\rightarrow i+1}$ the radial interface between the stem tissues i and i+1 [m^2], which is calculated from the stem dimensions.

In contrast to the vertical flows, the radial flows occur across a membrane and therefore follow a gradient in $\prod_j^i$ (Equation 2). $\prod_j^i$ is calculated according to the van't Hoff relationship (Jones, 1992; Génard *et al.*, 2001; Daudet *et al.*, 2002):

$$\prod_j^i = \frac{R(T+273)C_j^i}{MM_{sucrose}} \quad (4)$$

with R the universal gas constant [MJ mol^{-1} K^{-1}], T the temperature [°C], C_j^i the sucrose concentration [mg m^{-3}], and $MM_{sucrose}$ the molar mass of sucrose [mg mol^{-1}]. All osmotic components are expressed in sucrose equivalents, since sucrose is the predominant transport sugar in many species (Van Bel, 2003). The osmotic potential was neglected in the xylem since it is mostly <0.1 MPa (Jones, 1992).

The vertical and radial water flows induce changes in water content (W [mg]) which can be derived using a mass balance:

$$\frac{dW_j^i}{dt} = \sum F + \sum f \quad (5)$$

This equation is not valid for W_{stem}^X, W_{stem}^{Pc}, and W_{stem}^{Cz} due to irreversible growth as explained further. The model assumes that the xylem water content in the roots is fixed. This assumption is valid for young trees, since no important time lags could be detected between stem and root sap flow (Steppe and Lemeur, 2004). In the present study, it is also assumed that these time lags can be neglected for larger trees, such as T2.

Concept of dynamic carbon transport

Net photosynthesis (P_n) is used as input variable for the carbon transport submodel, because it indirectly determines the concentration-dependent loading of sucrose into the crown's phloem tubes. In these phloem tubes, a gradient in hydrostatic pressure drives the water flow and its corresponding mass flow of solutes (Münch, 1930):

$$S_j^{Pc} = \frac{C_j^{Pc} F_j^{Pc}}{\rho_w} \quad (6)$$

with S_j^{Pc} the sucrose transport rate in the phloem tubes [mg sucrose s^{-1}] and C_j^{Pc} the sucrose concentration in the phloem tubes of j (crown and stem) [mg sucrose m^{-3}].

The pressure gradient is set up by accumulation or loading of sucrose in the phloem tubes at the sites of production and a release or unloading of sucrose at the sites of consumption. The loading and unloading processes in the model are restricted to the crown and root compartment, respectively, since no vegetative or reproductive sinks are considered for T1 and T2. Sucrose is loaded from the storage cells (S) to the phloem tubes (Pc) in the crown compartment. This loading rate (L [mg sucrose s^{-1}]) is concentration dependent (Peuke *et al.*, 2001) and considered to obey simple Michaelis–Menten kinetics (Borstlap and Schuurmans, 2004):

$$L = V_{max,L} \frac{C_{crown}^S}{K_{M,L} + C_{crown}^S} \quad (7)$$

with C_{crown}^S the sucrose concentration in the storage tissue of the crown [mg m^{-3}], and $V_{max,L}$ [mg sucrose s^{-1}] and $K_{M,L}$ [mg m^{-3}] the kinetic parameters. The unloading rate in the roots (U [mg s^{-1}]) is concentration dependent, as suggested by Thompson and Holbrook (2003). However, in our model, the concentration set-point for unloading is replaced by the sucrose concentration of the storage tissue in the roots (C_{roots}^S [mg m^{-3}]):

$$U = k_U \frac{C_{roots}^{Pc}}{C_{roots}^S} \quad (8)$$

with C_{roots}^{Pc} the sucrose concentration in the phloem tubes of the roots [mg m^{-3}], and k_U the unloading rate when the sucrose concentration in the phloem tubes and the storage tissue is equal [mg s^{-1}].

Recently, the existence of lateral sugar flows was observed along the length of the transport phloem (Gould *et al.*, 2004, 2005). These lateral sugar flows are considered as a mechanism to ensure that short-term changes in solute supply do not limit sink development and that short-term changes in sink requirements are not detected by the sources (Gould *et al.*, 2004). The model considers this radial flow of sugar ($s_{stem}^{i\rightarrow i+1}$ [mg sucrose s^{-1}]) only in the stem compartment. Diffusion-like kinetics (Lacointe and Minchin, 2008) describe this exchange of sucrose between the phloem tubes and the adjacent tissues (i.e. the cambial zone and storage tissues):

$$s_{stem}^{i\rightarrow i+1} = k_{lat}^{i\rightarrow i+1}\left(C_{stem}^i - C_{stem}^{i+1}\right) \quad (9)$$

with $k_{lat}^{i\rightarrow i+1}$ a kinetic constant [m^3 s^{-1}] and i the cambial zone (Cz), phloem tubes (Pc), or storage tissues (S). It is assumed that no sucrose is transported towards the xylem vessels, since the osmotic potential of the xylem vessels is neglectable. In addition, all sugars are described in sucrose equivalents; therefore, the model cannot distinguish between the different sugar components.

Concept of stem diameter variations

As mentioned above, stem diameter variations consist of daily fluctuations (i.e. shrinkage and swelling) and irreversible radial stem growth. The daily fluctuations are solely

driven by the tissue water content and, hence, depend largely on the elasticity of the tissues (Hölttä *et al.*, 2006). When water leaves the tissue, its elasticity determines the magnitude of increase or decrease of tension or pressure, respectively. These elastic fluctuations are described by Hooke's law (Jones, 1992; Génard *et al.*, 2001; Hölttä *et al.*, 2006):

$$\frac{\mathrm{d}P_{\mathrm{j}}^{\mathrm{i}}}{\mathrm{d}t} = \frac{\epsilon_{\mathrm{j}}^{\mathrm{i}}\,\mathrm{d}W_{\mathrm{j}}^{\mathrm{i}}}{W_{\mathrm{j}}^{\mathrm{i}}\,\mathrm{d}t} \tag{10}$$

with $\epsilon_{\mathrm{j}}^{\mathrm{i}}$ the bulk elastic modulus of the tissue [MPa]. A high value of $\epsilon_{\mathrm{j}}^{\mathrm{i}}$ indicates an inelastic tissue. $\epsilon_{\mathrm{j}}^{\mathrm{i}}$ increases with turgor in the living tissues (Murphy and Ortega, 1995):

$$\epsilon_{\mathrm{j}}^{\mathrm{i}} = \epsilon_{\infty}\left(1 - e^{-7\left(P_{\mathrm{j}}^{\mathrm{i}} - 0.01\right)}\right) \tag{11}$$

with ε_{∞} the hypothetical maximum value when P reaches ∞ [MPa]. However, Equation 11 appeared not to be suitable for model calculations, because unrealistic negative values for $\epsilon_{\mathrm{j}}^{\mathrm{i}}$ were induced by negative $P_{\mathrm{j}}^{\mathrm{i}}$ which might accompany plasmolysis (Jones, 1992). A new relationship similar to Equation 11 was therefore established:

$$\epsilon_{\mathrm{j}}^{\mathrm{i}} = 0.001 + \frac{\epsilon_{\infty} - 0.001}{1 + e^{-20\left(P_{\mathrm{j}}^{\mathrm{i}} - 0.1\right)}} \tag{12}$$

It was assumed that $\epsilon_{\mathrm{j}}^{\mathrm{X}}$ of the xylem tubes was constant and was the same in crown, stem and roots.

In contrast to the daily fluctuations, the irreversible stem growth is related to both the water and the sugar content. Water will enter the growing cell to attain equilibrium in water potential. However, this extra amount of water results in an increase of turgor pressure and stress on the cell wall. When the turgor pressure exceeds a minimum value, stress relaxation of the cell wall will take place. As a result, turgor pressure will reduce, causing a new gradient in water potential (Lockhart, 1965). This reduction in P due to stress relaxation is exponential and dependent on wall rheological properties (Cosgrove, 1986):

$$\frac{\mathrm{d}P_{\mathrm{j}}^{\mathrm{i}}}{\mathrm{d}t} = -\epsilon_{\mathrm{j}}^{\mathrm{i}}\phi\left(P_{\mathrm{j}}^{\mathrm{i}} - \Gamma\right) \qquad \text{if } P_{\mathrm{j}}^{\mathrm{i}} > \Gamma \tag{13}$$

with Γ the threshold turgor [MPa] and φ the cell wall extensibility [$\mathrm{MPa}^{-1}\ \mathrm{s}^{-1}$]. In the model, irreversible structural growth is only considered in the cambial zone (i=Cz; j=stem) where cells divide, grow, and differentiate. From Equation 14, it can be derived that the decrease in $P_{\mathrm{j}}^{\mathrm{i}}$ will be larger when irreversible growth takes place (Génard *et al.*, 2001):

$$\frac{\mathrm{d}P_{\mathrm{stem}}^{\mathrm{Cz}}}{\mathrm{d}t} = \frac{\epsilon_{\mathrm{stem}}^{\mathrm{Cz}}}{W_{\mathrm{stem}}^{\mathrm{Cz}}}\frac{\mathrm{d}W_{\mathrm{stem}}^{\mathrm{Cz}}}{\mathrm{d}t} - \epsilon\phi\left(P_{\mathrm{stem}}^{\mathrm{Cz}} - \Gamma\right) \qquad \text{if } P_{\mathrm{stem}}^{\mathrm{Cz}} > \Gamma \tag{14}$$

$$\frac{\mathrm{d}P_{\mathrm{stem}}^{\mathrm{Cz}}}{\mathrm{d}t} = \frac{\epsilon_{\mathrm{stem}}^{\mathrm{Cz}}}{W_{\mathrm{stem}}^{\mathrm{Cz}}}\frac{\mathrm{d}W_{\mathrm{stem}}^{\mathrm{Cz}}}{\mathrm{d}t} \qquad \text{if } P_{\mathrm{stem}}^{\mathrm{Cz}} \leqslant \Gamma \tag{15}$$

The volume changes which drive the stem diameter variations are related to changes in water content (Equation 5):

$$\frac{\mathrm{d}V_{\mathrm{j}}^{\mathrm{i}}}{\mathrm{d}t} = \frac{1}{\rho_{\mathrm{w}}}\frac{\mathrm{d}W_{\mathrm{j}}^{\mathrm{i}}}{\mathrm{d}t} \tag{16}$$

with $V_{\mathrm{j}}^{\mathrm{i}}$ the tissue volume [m^3]. However, when irreversible growth takes place, not only does water uptake increase due to cell wall relaxation, but also the formation of new structural matter, which prevents the cell walls becoming thinner and weaker. To simulate this increase in structural matter, the model assumes that the volume fraction of water and dry matter remains constant during irreversible growth and that the synthesis of new matter appears simultaneous with cell relaxation (Cosgrove, 2005):

$$\text{if } P_{\mathrm{stem}}^{\mathrm{Cz}} > \Gamma \quad \frac{\mathrm{d}V_{\mathrm{stem}}^{\mathrm{Cz}}}{\mathrm{d}t} = \frac{1}{f_{\mathrm{stem}}^{\mathrm{Cz}}\rho_{\mathrm{w}}}\frac{\mathrm{d}W_{\mathrm{stem}}^{\mathrm{Cz}}}{\mathrm{d}t} \tag{17}$$

with $f_{\mathrm{stem}}^{\mathrm{Cz}}\left(=\frac{W_{\mathrm{stem}}^{\mathrm{Cz}}}{\rho_{\mathrm{w}}V_{\mathrm{stem}}^{\mathrm{Cz}}}\right)$ the fraction of water in the cambial zone [v/v] and $(1 - f_{\mathrm{stem}}^{\mathrm{Cz}})$ the dry matter fraction of the cambial zone [v/v].

In a real plant, the dimension of the cambial zone remains more or less constant, because mature cambial cells differentiate in either conductive xylem vessels or phloem tubes. Therefore, the model assumes that all new cambial cells differentiate to conductive xylem vessels (X) or phloem tubes (Pc) when the initial volume of the cambial zone is exceeded. Furthermore, the model assumes that xylem vessels are formed, elongated, and lignified in the cambial zone; afterwards they die and become conductive (X). As such, the volume increase in X is not described by reduction in P due to stress relaxation, but by an increase in the numbers of conduits formed in the cambial zone. The volume increase of the conductive phloem tubes (Pc) is described in a similar way. Since it is well known that the amount of xylem tissue formed in a single growing season is larger than that of the phloem tissue, the model assumes that the growing cells of the cambial zone differentiate 80% to xylem vessels and 20% to phloem tubes:

if $V_{\mathrm{stem}}^{\mathrm{Cz}} > V_{\mathrm{stem,int\,ial}}^{\mathrm{Cz}}$ and $P_{\mathrm{stem}}^{\mathrm{Cz}} > \Gamma$

$$\frac{\mathrm{d}V_{\mathrm{stem}}^{\mathrm{Cz}}}{\mathrm{d}t} = 0 \tag{18}$$

$$\frac{\mathrm{d}V_{\mathrm{stem}}^{\mathrm{Pc}}}{\mathrm{d}t} = \frac{1}{\rho_{\mathrm{w}}}\left((\Sigma F(\mathrm{Pc}) + \Sigma f(\mathrm{Pc})) + \frac{1}{f_{\mathrm{w}}}0.2(\Sigma F(\mathrm{Cz}) + \Sigma f(\mathrm{Cz}))\right) \tag{19}$$

$$\frac{\mathrm{d}V_{\mathrm{stem}}^{\mathrm{X}}}{\mathrm{d}t} = \frac{1}{\rho_{\mathrm{w}}}\left((\Sigma F(\mathrm{X}) + \Sigma f(\mathrm{X})) + \frac{1}{f_{\mathrm{w}}}0.8(\Sigma F(\mathrm{Cz}) + \Sigma f(\mathrm{Cz}))\right) \tag{20}$$

The same proportions need to be taken into account to have a valid mass balance of water:

If $V_{\mathrm{stem}}^{\mathrm{Cz}} > V_{\mathrm{stem,int\,ial}}^{\mathrm{Cz}}$ and $P_{\mathrm{stem}}^{\mathrm{Cz}} > \Gamma$

$$\frac{\mathrm{d}W_{\mathrm{stem}}^{\mathrm{Cz}}}{\mathrm{d}t} = 0 \tag{21}$$

$$\frac{\mathrm{d}W_{\mathrm{stem}}^{\mathrm{Pc}}}{\mathrm{d}t} = (\Sigma F(\mathrm{Pc}) + \Sigma f(\mathrm{Pc})) + 0.2(\Sigma F(\mathrm{Cz}) + \Sigma f(\mathrm{Cz})) \tag{22}$$

$$\frac{\mathrm{d}W_{\mathrm{stem}}^{\mathrm{X}}}{\mathrm{d}t} = (\Sigma F(\mathrm{X}) + \Sigma f(\mathrm{X})) + 0.8(\Sigma F(\mathrm{Cz}) + \Sigma f(\mathrm{Cz})) \tag{23}$$

The stem is the only compartment which contains a cambial zone, since the model aims to simulate stem growth and not root nor leaf growth.

The variations in stem diameter are equal to the variations in diameter of the outer coaxial cylinder ($D_{\mathrm{stem}}^{\mathrm{S}}$ [m]) (Fig. 1). However, to calculate this diameter, the diameter of all the other inner coaxial cylinders has to be determined:

$$D_{\mathrm{stem}}^{\mathrm{i}} = \sqrt{\left(D_{\mathrm{stem}}^{\mathrm{i-1}}\right)^2 + \frac{4V_{\mathrm{stem}}^{\mathrm{i}}}{\pi l}} \tag{24}$$

with $D_{\mathrm{stem}}^{\mathrm{i}}$ the diameter of the coaxial cylinder which represents the tissue i of the stem compartment [m] and with l the length of the stem [m]. It is assumed that the heartwood will not change in volume or water content, since it is not actively participating in water and sugar transport.

Concept of respiration and starch conversion

In order to complete the carbon balance, the model considers maintenance respiration and starch conversion in the storage tissues (S) of the roots, the stem, and the crown. The conversion of excess sugars to starch ($\mathrm{St}_{\mathrm{j}}^{\mathrm{S}}$ [mg]) is driven by a target sucrose concentration in the storage tissues (C_0 [mg m^{-3}]) (Daudet *et al.*, 2002; Lacointe and Minchin, 2008):

$$\frac{\mathrm{dSt}_{\mathrm{j}}^{\mathrm{S}}}{dt} = k_{\mathrm{starch}}\left(C_{\mathrm{j}}^{\mathrm{S}} - C_0\right) \tag{25}$$

with k_{starch} a kinetic parameter [m^3 s^{-1}]. C_0 is set equivalent to an osmotic pressure Π_0 [MPa].

The maintenance respiration ($\mathrm{Rm}_{\mathrm{j}}^{\mathrm{S}}$ [mg sucrose s^{-1}]) is proportional to the living biomass of the tissue and to the sucrose concentration (Daudet *et al.*, 2002; Lacointe and Minchin, 2008):

$$\mathrm{Rm}_{\mathrm{j}}^{\mathrm{S}} = \left(k_{\mathrm{Rm,1}} + k_{\mathrm{Rm,2}}C_{\mathrm{j}}^{\mathrm{S}}\right)\left(1 - f_{\mathrm{j}}^{\mathrm{S}}\right)V_{\mathrm{j}}^{\mathrm{S}} \tag{26}$$

with $k_{\mathrm{Rm,1}}$ [mg sucrose m^{-3} s^{-1}] and $k_{\mathrm{Rm,2}}$ [s^{-1}] kinetic parameters. Maintenance respiration is, however, not explicitly calculated in the storage tissue of the crown, since the measured net photosynthesis takes into account both gross photosynthesis and respiration.

In the cambial zone of the stem, both maintenance and growth respiration are considered. The growth respiration ($\mathrm{Rg}_{\mathrm{stem}}^{\mathrm{Cz}}$ [mg sucrose s^{-1}]) is modelled using the concept of Thornley (Le Roux *et al.*, 2001) who introduced the growth efficiency or yield (Y [dimensionless]):

$$\mathrm{Rg}_{\mathrm{stem}}^{\mathrm{Cz}} = \left(\frac{1}{Y} - 1\right)\frac{1}{f_{\mathrm{stem}}^{\mathrm{Cz}}\rho_{\mathrm{w}}}(\Sigma F(\mathrm{Cz}) + \Sigma f(\mathrm{Cz}))\rho_{\mathrm{wood}}1.13 \tag{27}$$

with ρ_{wood} the density of dry wood [mg m^{-3}] equal to 0.75×10^9 (Forsythe, 1954;2003) and the value 1.13 [mg sucrose mg^{-1} wood] derived from the carbon content in wood (i.e. ~47.5%) (Thomas and Malczewski, 2007). The carbon balance could be calculated by taking into account starch conversion, respiration, structural growth, and carbon transport:

$$\frac{\mathrm{dM}_{\mathrm{crown}}^{\mathrm{S}}}{\mathrm{d}t} = P_{\mathrm{n}}\frac{\mathrm{MM}_{\mathrm{sucrose}}}{12} - L - \frac{\mathrm{dSt}_{\mathrm{crown}}^{\mathrm{S}}}{\mathrm{d}t} \tag{28}$$

$$\frac{\mathrm{dM}_{\mathrm{stem}}^{\mathrm{S}}}{\mathrm{d}t} = -\mathrm{Rm}_{\mathrm{stem}}^{\mathrm{S}} + \mathrm{S}_{\mathrm{stem}}^{\mathrm{PcS}} - \frac{\mathrm{dSt}_{\mathrm{crown}}^{\mathrm{S}}}{\mathrm{d}t} \tag{29}$$

$$\frac{\mathrm{dM}_{\mathrm{stem}}^{\mathrm{Cz}}}{\mathrm{d}t} = -\mathrm{Rm}_{\mathrm{stem}}^{\mathrm{Cz}} - \frac{\mathrm{Rg}_{\mathrm{stem}}^{\mathrm{Cz}}}{1-Y} + s_{\mathrm{stem}}^{\mathrm{CzPc}} \tag{30}$$

$$\frac{\mathrm{dM}_{\mathrm{roots}}^{\mathrm{S}}}{\mathrm{d}t} = -\mathrm{Rm}_{\mathrm{roots}}^{\mathrm{S}} - U - \frac{\mathrm{dSt}_{\mathrm{roots}}^{\mathrm{S}}}{\mathrm{d}t} \tag{31}$$

$$\frac{\mathrm{dM}_{\mathrm{j}}^{\mathrm{Pc}}}{\mathrm{d}t} = \sum S_{\mathrm{j}}^{\mathrm{Pc}} + \sum s_{\mathrm{j}}^{\mathrm{i}\rightarrow\mathrm{i+1}} \tag{32}$$

Model implementation

The model, consisting of a set of algebraic and differential equations, is solved numerically using the homemade modelling and simulation software package STACI (Steppe *et al.*, 2008). This environment allows simulation, calibration, sensitivity analysis, identifiability analysis, and data acquisition.

Initial values for variables and parameters

The initial values of $W_{\mathrm{j}}^{\mathrm{i}}$ were derived from the initial values of $D_{\mathrm{stem}}^{\mathrm{i}}$ and $V_{\mathrm{j}}^{\mathrm{i}}$ which were estimated from measurements. The stem anatomy of T1 was studied and used to estimate $W_{\mathrm{j}}^{\mathrm{i}}$ (Table 4). Transverse sections were cut from stem samples of T1 with a sliding microtome. These sections were dehydrated, embedded in paraffin, stained with astrablue/safranine, and mounted in Euparal. Afterward, a binocular microscope was used to measure the width of the cambial zone (Cz), conducting secondary phloem (Pc), and non-conducting phloem/cortex (S). The same stem samples revealed that the entire xylem tissue was conductive ($D_{\mathrm{stem}}^{\mathrm{H}}$=0. Furthermore, the total stem diameter ($D_{\mathrm{stem}}^{\mathrm{S}}$) and bark width were measured with a sliding calliper. Such a detailed anatomical study could not be performed on T2. Instead, microcores from the stem of T2 were taken to determine the depth of sapwood and heartwood, while the bark thickness was measured with a calliper. The width of Cz and Pc of T2 was calculated by assuming that the

Table 4. (A) Initial values for variables derived from experimental measurements for both growth chamber (T1) and forest (T2) conditions; (B) Estimated values for parameters after model calibration for T1 and T2 in comparison with literature values

Note that some of the presented literature values are the result of a calculation with values found in the literature to obtain the same parameter unit.

Symbol	Unit	T1	T2	
A. Variable				**Measurement**
D^{H}_{stem}	[m]	0	0.139	Stem anatomy
D^{X}_{stem}	[m]	1.685×10^{-2}	0.4056	Stem anatomy
D^{Cz}_{stem}	[m]	1.700×10^{-2}	0.4063	Stem anatomy
D^{Pc}_{stem}	[m]	1.740×10^{-2}	0.4086	Stem anatomy
D^{S}_{stem}	[m]	1.950×10^{-2}	0.4170	Stem anatomy
l	[m]	1	14	Stem anatomy
LA	[m^2]	0.5346	426.2867	Leaf area
$V^{X}_{crown} = V^{X}_{roots}$	[m^3]	1.710×10^{-6}	682×10^{-6}	Leaf area
$V^{Pc}_{crown} = V^{Pc}_{roots}$	[m^3]	0.428×10^{-6}	171×10^{-6}	Leaf area
$V^{S}_{crown} = V^{S}_{roots}$	[m^3]	532×10^{-6}	425 434×10^{-6}	Leaf area
ψ_{soil}	[MPa]	–0.0037	–0.04	Tensiometer
B. Parameter				**Literature value (References)**
Π_0*	[MPa]	0.98	1	1 (Jones, 1992)
Γ	[MPa]	0.895	1.235	0.2–0.9 (Cosgrove, 1986; Frensch and Hsiao, 1995; Génard *et al.*, 2001; Steppe *et al.*, 2006*a*)
Y	[dimensionless]	0.75	0.7	0.6–0.9 (Le Roux *et al.*, 2001)
φ	[MPa^{-1} s^{-1}]	8.6×10^{-5}	6.0×10^{-6}	9 10^{-5}–2.3×10^{-7} (Cosgrove, 1986; Hsiao *et al.*, 1998; Génard *et al.*, 2001; Steppe *et al.*, 2006*a*)
R^{X}*	[MPa s mg^{-1}]	0.075	0.00012	0.18–1.5×10^{-3} (Hölttä *et al.*, 2006; Steppe *et al.*, 2006*b*; Lacointe and Minchin, 2008)
$k^{Cz\rightarrow S}_{lat}$	[m^3 s^{-1}]	1.3×10^{-9}	8.1×10^{-7}	
$V_{max,L}$	[mg sucrose s^{-1}]	0.12	30	T1: 0.02–0.03 (Borstlap and Schuurmans, 2004) T2: 15–26
k_U	[mg s^{-1}]	0.048	26	
ϵ^{S}_{∞} *	[MPa]	8.5	40	1–50 (Murphy and Ortega, 1995; Backes and Leuschner, 2000)
$R^{X\rightarrow Pc}_{roots}$	[MPa s mg^{-1}]	0.07	0.008	
$R^{X\rightarrow Pc}_{crown}$*	[MPa s mg^{-1}]	1.01	0.024	
R^{Pc}	[MPa s mg^{-1}]	0.09	0.0008	0.01–3.6 (Hölttä *et al.*, 2006; Lacointe and Minchin, 2008)
L_{rad}*	[m MPa^{-1} s^{-1}]	1.0×10^{-6}	7.7×10^{-8}	10^{-4}–10^{-7} (Hölttä *et al.*, 2006; Steppe *et al.*, 2006*a*)
k_{starch}*	[m^3 s^{-1}]	2.6×10^{-7}	4.6×10^{-4}	10^{-3} (Daudet *et al.*, 2002)
ϵ^{Pc}_{∞}	[MPa]	10	70	1–50 (Lee, 1981; Jones, 1992)
ϵ^{X}*	[MPa]	1021	1350	900–1500 (Irvine and Grace, 1997; Hölttä *et al.*, 2006)
$k^{Pc\rightarrow S}_{lat}$*	[m^3 s^{-1}]	3.9×10^{-10}	6.1×10^{-8}	
$K_{M,L}$	[mg m^{-3}]	1.61×10^{8}	7 10^{6}	1.2×10^{6} (Borstlap and Schuurmans, 2004)
$k_{Rm,1}$	[mg sucrose m^{-3} s^{-1}]	533	233	833 (Daudet *et al.*, 2002)
$k_{Rm,2}$*	[s^{-1}]	2.4×10^{-7}	5.1×10^{-8}	2.43×10^{-7} (Daudet *et al.*, 2002)

* The parameter values were determined by automatic calibration.

diameter ratios of the different tissues were similar to T1. Afterwards, W^{i}_{stem} could be calculated from D^{i}_{stem} by taking into account the stem length (l) and a water fraction of 50% in the stem (Tyree, 1988; Peramaki *et al.*, 2001). The total volume of the crown was estimated from the leaf thickness (~1 mm) and the measured leaf area (Table 4). Furthermore, a leaf vein density of 2 mm mm^{-2} (Salleo *et al.*, 2003) was assumed and a phloem/xylem ratio of 1/4 in the veins. Since no measurements were performed on the root compartment, the root tissue volumes were set equal to the volumes of the crown. W^{i}_{crown} and W^{i}_{roots} could be calculated from these volumes by taking into account a water fraction of 85% and 50% in leaves and roots, respectively (Jones, 1992).

All simulations were started at the end of the night when steady-state conditions were reached in the tree. By assuming these steady-state conditions, the initial values of the variables P^{i}_{j} and $\prod^{i}_{j}$ could be derived for all compartments. The steady-state conditions are described by several assumptions:

(i) there is no exchange with the environment: $E{=}P_n{=}F^{X}_{roots} = 0$

(ii) the lateral sugar flows are neglected in the stem compartment: $s^{Cz\rightarrow Pc}_{stem} = s^{Cz\rightarrow Pc}_{stem} = 0 \Rightarrow L = U$

(iii) respiration is neglected: Rg=Rm=0

(iv) no changes in water content (since $E{=}F^{X}_{roots} = 0$): $\frac{dW}{dt} = 0$

(v) starch conversion is in equilibrium in all storage tissues: $C_j^S = C_0$

(vi) the sugar concentrations in the cambial zone and the conductive phloem tubes are equal: $C_{stem}^{Cz} = C_{stem}^{Pc}$

Solving the mass balances for water and sugar under these conditions resulted in a set of equations to calculate P_j^i and $\prod_j^i$. The set of equations could not be solved explicitly; therefore, the solution was found using an iterative approach (Supplementary data available at *JXB* online).

The input variables of the model were the continuously measured data from E, P_n, and T.

Sensitivity analysis and identifiability analysis

A mathematical sensitivity and identifiability analysis was performed as described by De Pauw *et al.* (2008). These analyses were performed on the remaining parameters of which the value could not be estimated from measurements. The mean square criterion (δ_j^{msqr}) was calculated from a local sensitivity analysis. Large values of δ_j^{msqr} indicate a sensitive parameter j, whereas the opposite holds for low values of δ_j^{msqr}. The identifiability analysis was performed by taking into account that measurements of D_{stem}^S, F_{stem}^X, P_{crown}^X, and P_{stem}^X were available. From the identifiability analysis, the collinearity index (γ) was calculated for all possible subsets of the selected parameters. If γ is <15, the correlation between the parameters is considered low. A parameter set is found to be identifiable if its γ is <15 and the sum of sensitivities of the individual parameters is high (De Pauw *et al.*, 2008).

Model simulation and calibration

For simulations a fourth-order Runge–Kutta numerical integrator with adaptive step size was used (integrator settings: accuracy: 1×10^{-6} and maximum step size=0.1). Model calibration was performed by using the simplex method (Nelder and Mead, 1965) which was one of the search algorithms implemented in STACI.

Results and Discussion

Model sensitivity and identifiability

Table 5 shows the results of the sensitivity analysis of the 20 remaining model parameters which could not be estimated from performed measurements. Regarding D_{stem}^S, the parameters could be subdivided into three groups. A first group contained five highly sensitive parameters: Π_0 which is related to the calculation of initial values, $V_{max,L}$ and $K_{M,L}$ which are related to the loading rate, k_U which is related to the unloading rate, and Γ which is related to radial stem growth. In addition, a group of seven parameters of medium sensitivity and one of eight parameters of low sensitivity could be distinguished. The variables F_{stem}^X, P_{stem}^X, and P_{crown}^X were relatively sensitive to R^X, while F_{stem}^{Pc} was mostly sensitive to k_U (Table 5). The identifiability analysis showed that the model had identifiability problems, since no parameter subset of ⩾10 had a collinearity index <15 (Table 6). A subset of only nine model parameters was therefore selected for further automatic calibration. The selected subset contained the parameters: Π_0, R^X, ϵ_∞^S, L_{rad}, k_{starch}, $k_{Rm,2}$, $k_{lat}^{Cz\to S}$, $R_{crown}^{X\to F}$, and ϵ^X. This subset showed the highest sensitivity (δ_j^{msqr} (total)= 1589)

Table 5. Sensitivity indices of the 20 remaining parameters of which the value could not be estimated from measurements

Parameter	δ_j^{msqr} (D_{stem}^S)	δ_j^{msqr} (F_{stem}^X)	δ_j^{msqr} (P_{stem}^X)	δ_j^{msqr} (P_{crown}^X)	δ_j^{msqr} (F_{stem}^{Pc})
Π_0	2425.8	7.0	0.2	0.7	2.2
$V_{max,L}$	1653.6	1.7	0.0	0.1	0.5
k_U	1542.3	1.2	0.0	0.1	2.4
Γ	1309.1	1.1	0.0	0.0	0.1
$K_{M,L}$	892.9	0.9	0.0	0.1	0.3
φ	162.6	0.2	0.0	0.0	0.0
R^X	131.8	14.5	6.4	12.3	1.3
R^{Pc}	36.5	0.0	0.0	0.0	0.1
$k_{lat}^{Cz\to S}$	36.1	0.1	0.0	0.0	0.0
Y	34.4	0.2	0.0	0.1	0.0
$R_{roots}^{X\to Pc}$	28.3	0.0	0.0	0.0	0.0
ϵ_∞^S	21.6	1.5	0.0	0.1	0.0
$k_{Rm,1}$	10.3	0.1	0.0	0.1	0.0
K_{starch}	3.9	0.2	0.0	0.0	0.0
L_{rad}	3.0	0.6	0.0	0.0	0.0
$R_{crown}^{X\to Pc}$	3.0	5.9	0.1	0.6	0.0
$k_{Rm,2}$	1.8	0.1	0.0	0.1	0.0
ϵ_∞^{Pc}	1.6	0.1	0.0	0.0	0.0
ϵ^X	0.8	0.1	0.0	0.0	0.0
$k_{lat}^{Pc\to S}$	0.6	0.1	0.0	0.0	0.0

Table 6. Total number of subsets of different sizes considered during the identifiability analysis

Subset size	Total number	Number with γ <15
2	190	135
3	1140	480
4	4845	1050
5	15 504	1502
6	38 760	1409
7	77 520	841
8	125 970	290
9	167 960	44
10	184 756	0
11	167 960	0
12	125 970	0
13	77 520	0
14	38 760	0
15	15 504	0
16	4845	0
17	1140	0
18	190	0
19	20	0
20	1	0

and had a collinearity index <15 (γ=10.7). In addition, the identifiability analysis revealed that the two parameters with the highest sensitivity, Π_0 and k_U (Table 5), were highly correlated. These parameters had the highest correlation index of all two-parameter subsets (γ=2497).

Simulation and calibration

Large differences existed between PAR and model inputs (T, E, and P_n) used for T1 and T2, respectively (Fig. 2). The meteorological variables PAR and T were controlled to be a step function in the growth chamber of T1 (Fig. 2A, B). These conditions caused the regular pattern in E and P_n, since the stomata of T1 were subjected to a constant light intensity and vapour pressure deficit during the daytime. In the case of T2, the microclimatic variables depended on the natural weather conditions in the forest, resulting in higher values and more irregular patterns (Fig. 2).

Using these input variables (Fig. 2) and the initial parameters (Table 4), the model was calibrated for the above selected subset of nine model parameters. The parameter values minimizing the sum of squared errors function (Table 4) were used for further model simulations. Values of the non-identifiable parameters were taken from the literature. If no literature values were available, a value was selected based on expert knowledge (Table 4). For example, the loading and unloading parameters ($V_{max,L}$, $K_{M,L}$, and k_U) were estimated from photosynthesis measurements by assuming that after 1 d or 2 d the net accumulation of starch was zero in the leaves.

After calibration, a good agreement was found between the simulated and measured values of D^S_{stem}, D^X_{stem}, F^X_{stem},

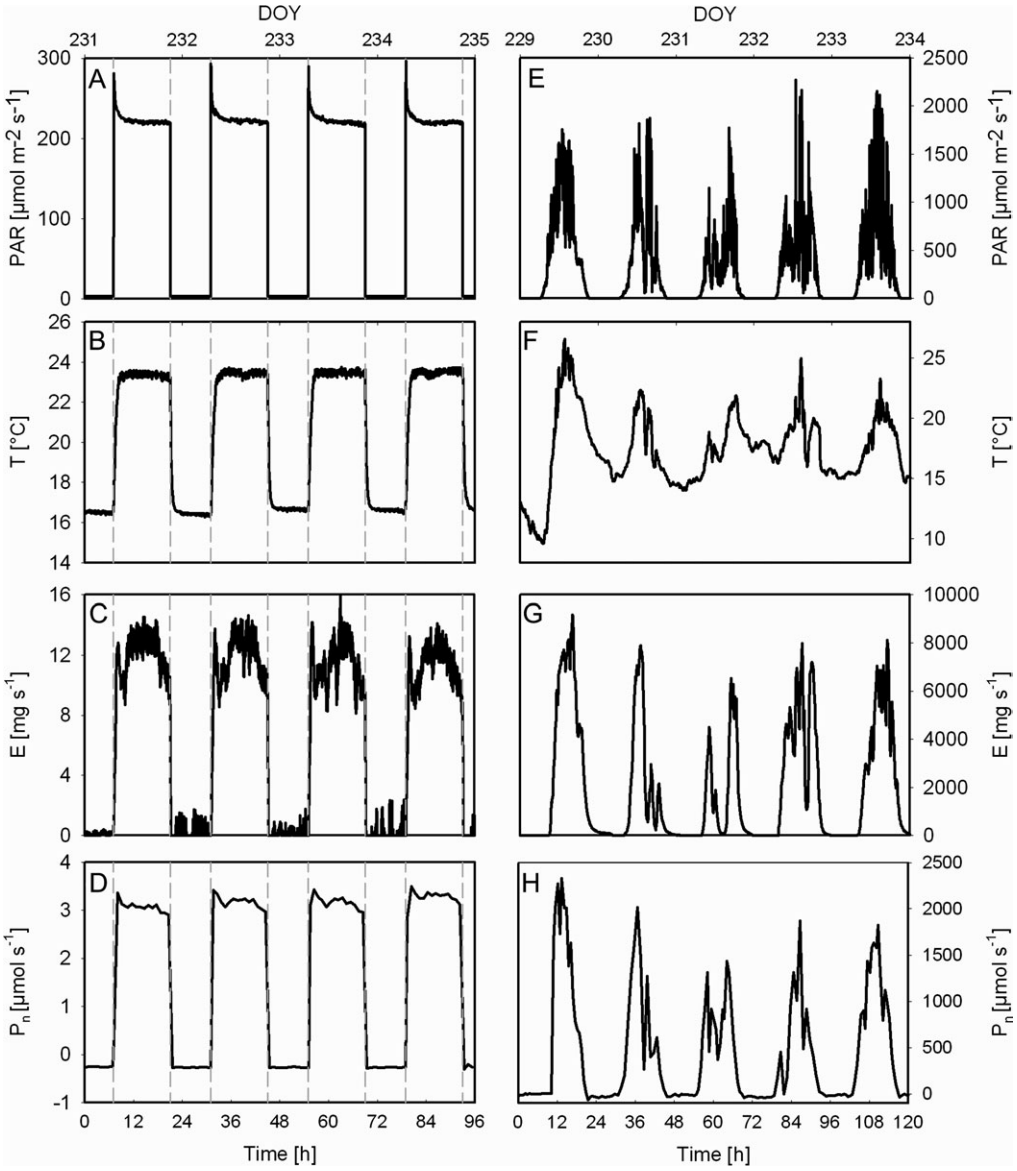

Fig. 2. The meteorological conditions [light regime (PAR) and temperature (T)] and the measurements used as model inputs [transpiration (E) and net photosynthesis (P_n)] for both the young oak tree in the growth chamber (T1) (A–D) and the adult beech tree in the forest (T2) (E–H) (DOY, day of year).

P^X_{crown}, and P^X_{stem} for both T1 and T2 (Fig. 3). D^S_{stem} decreased during the morning and increased during the evening. In addition, radial stem growth was observed and simulated (Fig. 3 A, E). A comparison between measurements and simulations for D^X_{stem} could only be made for T2 (Fig. 3F). This was not possible for T1, since no D^X_{stem} measurements were available (Fig. 3B). To simulate D^X_{stem}, the parameter Γ was set arbitrarily to 100 MPa to eliminate irreversible growth from the model simulation as no growth was observed in the actual xylem LVDT measurements. The simulation revealed that D^X_{stem} was mainly determined by ϵ^X (data not shown), which was also suggested by Hölttä *et al.* (2006). The values of F^X_{stem} were well simulated during the daytime (Fig. 3C, G). However, the night-time values of F^X_{stem} were slightly overestimated by the simulation. This discrepancy might be attributed to the measurement method of F^X_{stem}, since both the TDP and HB method assume zero flow conditions during the night in their calculation method. During the night, a non-zero sap flow (Hölttä *et al.*, 2006) was simulated in the xylem tissue due to the non-stop loading in the phloem tissue and the hydraulic link between xylem vessels and phloem tubes in the model. This night-time sap flow is called Münch's counterflow. Hence, a zero night-time sap flow condition can never been fulfilled in such a situation. However, no study so far exists in the literature about the impact of this Münch's counterflow on HB and TDP sensors. The water potential in the leaves (P^X_{crown}) was always lower than that in the stem (P^X_{stem})

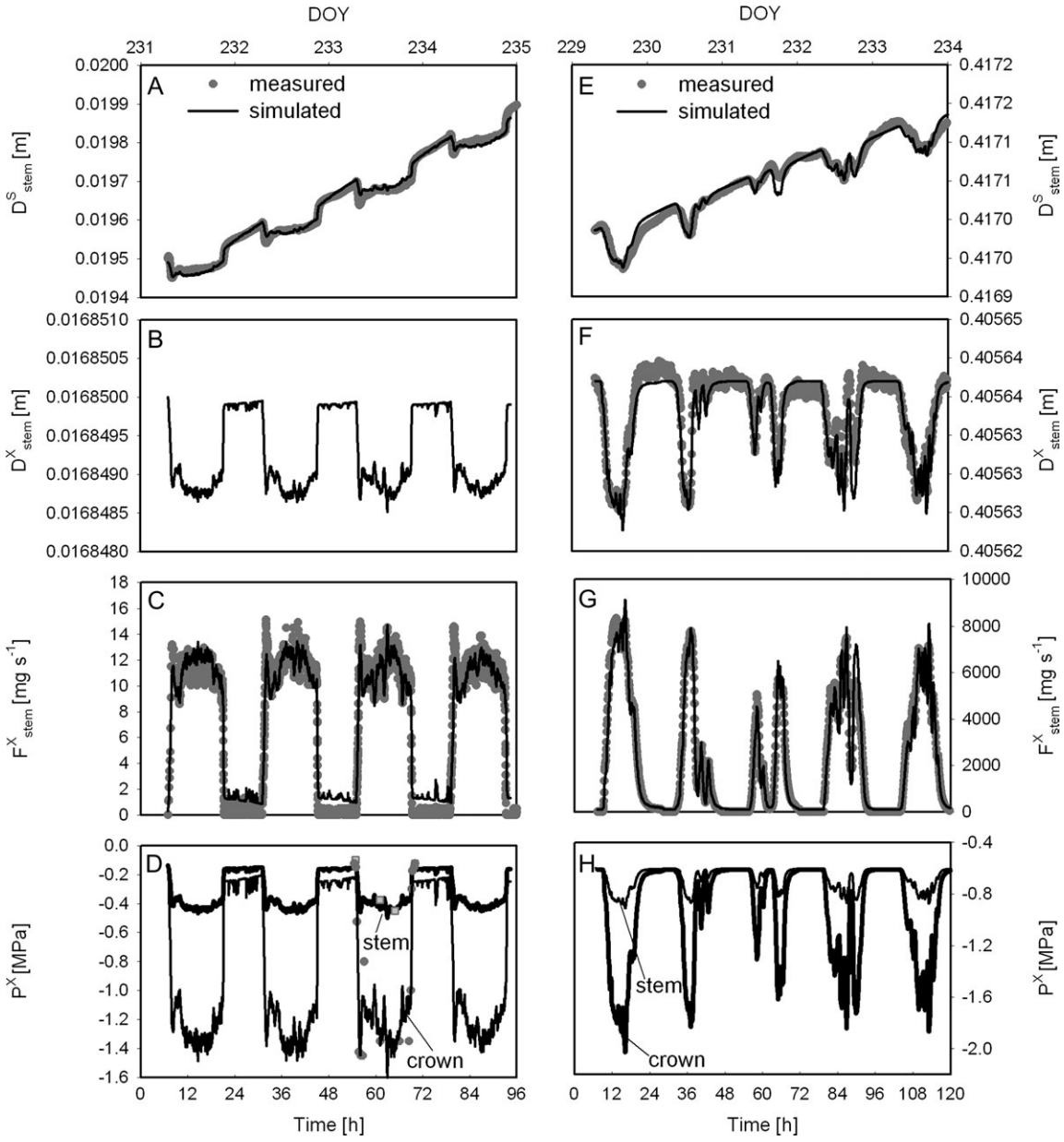

Fig. 3. Comparison between simulated and measured data of total stem diameter (D^S_{stem}), xylem stem diameter (D^X_{stem}), xylem sap flow in the stem (F^X_{stem}), xylem leaf water potential (P^X_{crown}), and xylem stem water potential (P^X_{stem}) for both the young oak tree in the growth chamber (T1) (A–D) and the adult beech tree in the forest (T2) (E–H) (DOY, day of year).

(Fig. 3D, H). The simulated leaf and stem water potentials corresponded well with the measurements for T1 (Fig. 3D). For T2, no water potential measurements were available during the simulated period. However, the simulated leaf water potentials were within the range reported in the literature for a similar beech: –1.61±0.33 MPa (Roberts and Rosier, 1994) (Fig. 3H). In conclusion, comparison between simulated and measured data revealed that the model simulated the tree water relations well (F^{X}_{stem}, P^{X}_{crown}, and P^{X}_{stem}) and indicated that the model was capable of simulating the sugar relations in a realistic way (D^{S}_{stem}).

Selected parameter values

The assigned parameter values mostly corresponded to literature values (Table 4). The values of Π_0 (Table 4) were close to the osmotic potential (1 MPa) of typical cell sap from many plants (Jones, 1992). The two growth parameters, Γ and φ, which are difficult to measure experimentally, revealed a higher growth rate of the cambial zone in T1. This difference might be attributed to the difference in age and/or genus of both trees, although the difference in microclimate (especially air temperature) might play an additional role (Perez-Lopez *et al.*, 2008). The value of φ was similar to measured values for cell wall extensibility, ranging from 4.5×10^{-6} to 9.0×10^{-5} (Cosgrove, 1986; Hsiao *et al.*, 1998). In the models of Génard *et al.* (2001) and Steppe *et al.* (2006), the estimated values of φ were one order of magnitude higher compared with the experimental values of Hsiao *et al.* (1998). In our model, radial growth was driven by growth in the cambial zone which continuously differentiated in xylem vessels and phloem tubes, while this tissue differentiation was not incorporated either in the model of Génard *et al.* (2001) or in the model of Steppe *et al.* (2006). Therefore, it can be concluded that more realistic simulations are obtained when the stem is considered to consist of different tissues with different growing behaviour. It is noteworthy that R^{X} of T1 was higher than that of T2. This difference followed from simulation of realistic leaf water potentials in both T1 and T2. Furthermore, in both instances, R^{X} was lower than R^{Pc}, which is logical since sieve plates in the phloem tubes cause a higher resistance which is absent in the xylem vessels. $R^{X\rightarrow Pc}_{roots}$ was lower than $R^{X\rightarrow Pc}_{crown}$ for both T1 and T2, suggesting a higher distribution of aquaporins in the unloading zones compared with the loading zone. All tissues of T1 were more elastic compared with T2, indicating that elasticity might decrease when tissues grow and increase in volume (Table 4).

Advantage of considering a hydraulic coupling between water and sugar transport in whole-tree models

The tree model was able to simulate sugar-related physiological variables which are difficult to measure (Fig. 4). A small pressure gradient existed in the phloem tissue (Fig. 4A, E), but was sufficient to transport the newly assimilated sugars from the crown to the roots. Thompson *et al.* (2006) also suggested that the sieve tube axial pressure is relatively small because a local drop in pressure could then be rapidly transmitted over long distances. A pressure gradient of 0.03 MPa m^{-1} has been observed by direct measurement of sieve element turgor pressure in mature oak trees (Hammel, 1968; Pritchard, 2007). This measured gradient corresponds to the simulations of T1 (0.042 MPa m^{-1} which is calculated as $\frac{P^{Pc}_{crown}-P^{Pc}_{roots}}{l}$); however, it is an overestimation when using the simulations of T2 (0.009 MPa m^{-1}). The simulated phloem pressures are in accordance with the literature values ranging from 0.8 MPa to 1.5 MPa (Hammel, 1968; Sovonick-Dunford *et al.*, 1981; Gould *et al.*, 2004, 2005; Pritchard, 2007). The simulations show that P^{Pc}_{crown} suddenly decreased in the morning when transpiration started because phloem water had to contribute to the transpiration stream (Fig. 4A, E). Some experimental studies have also observed such a daily dynamic, resulting from a transpiration effect (Peel and Weatherley, 1962; Sovonick-Dunford *et al.*, 1981; Pritchard, 2007).

A second effect of transpiration was the decrease in phloem water flow ($<F^{Pc}_{stem}$) during the daytime (Fig. 4B, F). Similar dynamics were simulated by the model of Hölttä *et al.* (2006). However, actual measurements of this behaviour are rare (Peuke *et al.*, 2001; Windt *et al.*, 2006). If measured, the behaviour is often judged insignificant and inconsistent, and it is therefore concluded that no significant differences exist between daytime and night-time phloem flow. This discrepancy between experimental and modelling studies might be provoked by a mechanism not yet included in the current models. According to Windt *et al.* (2006), such a mechanism could be an increased flow-conducting area of the phloem tissue during the night or the regulation of the phloem flow by modulating phloem sugar concentrations not only in sources and sinks, but also along the length of transport phloem.

The sugar transport towards the roots (S^{Pc}_{stem}) changed in agreement with F^{Pc}_{stem}, which was similar to the simulations obtained by Hölttä *et al.* (2006) (Fig. 4B, F). Furthermore, S^{Pc}_{stem} was nearly identical to the unloading rate (U), indicating that there was almost no sugar accumulation in the root phloem tissue. The loading rate (L) remained more or less constant, while U fluctuated daily around the loading rate (Fig. 4B, F).

During the daytime, the osmotic pressure (Π^{Pc}) increased in both the stem and crown phloem tissue (Fig. 4C, G), since L was larger than S^{Pc}_{stem}, causing a net accumulation of sucrose. In addition, the water content in the phloem tissue decreased due to the transpiration stream, leading to an additional increase in osmotic pressure. Surprisingly, the opposite dynamic was simulated in the roots (Fig. 4C, G). The roots received fewer sugars from the crown, because F^{Pc}_{stem} decreased. Although U also decreased, its decrease seemed not enough to counteract the decrease in phloem root osmotic potential. The model of Hölttä *et al.* (2006) simulated a similar opposite behaviour; however, not between stem and roots, but between the middle and top of the model tree. The simulated osmotic pressures in the phloem tissue were more or less within the range reported in the literature: $\prod^{Pc}_{roots}$=1–2 MPa (Pritchard, 2007), $\prod^{Pc}_{stem}$=1.8 MPa (Sovonick-Dunford *et al.*, 1981), $\prod^{Pc}_{crown}$=2–3 MPa

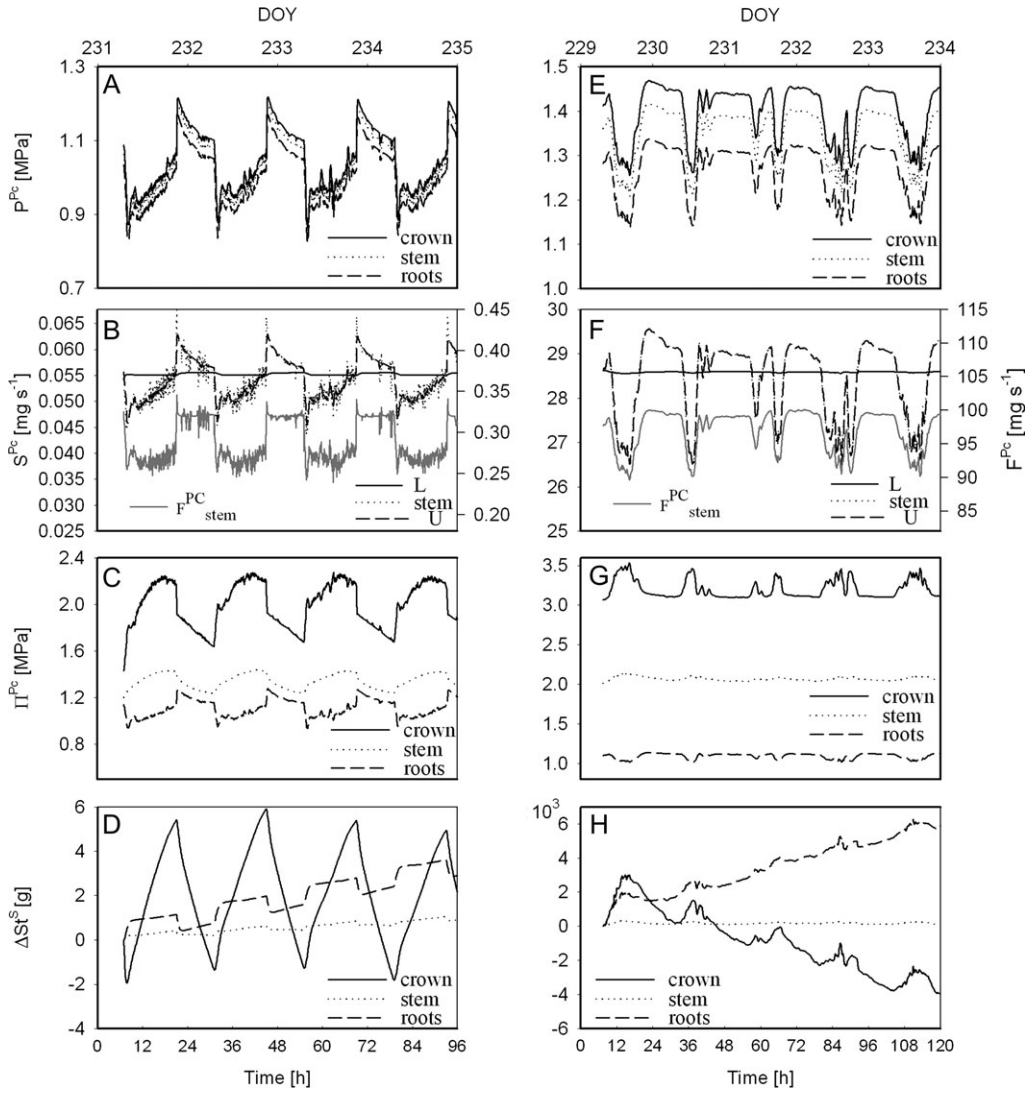

Fig. 4. Model simulations of turgor pressure (P^{Pc}), of water (F^{Pc}) and sugar (S^{Pc}) flows with the loading (L) and unloading (U) rates, of osmotic pressure (Π^{Pc}) in the phloem tubes; and of the change in starch content (ΔSt^{S}) for both the young oak tree in the growth chamber (T1) (A–D) and the adult beech tree in the forest (T2) (E–H) (DOY day of year).

(Gould *et al.*, 2005). Daily dynamics in osmotic pressure were also simulated by the models of Daudet *et al.* (2002) and Hölttä *et al.* (2006); sometimes they were measured (Peuke *et al.*, 2006; Windt *et al.*, 2006) and sometimes not (Sovonick-Dunford *et al.*, 1981). Due to the daily dynamics in Π^{Pc}, the axial gradient in Π^{Pc} is larger during the day compared with the night-time. This Π^{Pc} gradient was higher for the adult field-grown tree (T2) compared with the young tree grown under controlled conditions (T1), which is realistic since the distance between sources and sinks was much larger in the adult tree.

Starch accumulated in the leaves during the daytime and was depleted during the night-time (Fig. 4D, H). Due to this process of starch accumulation and depletion, loading and sugar transport in the phloem were possible without concomitant photosynthetic activity (Fig. 4B, F). The measurements of Peuke *et al.* (2001) suggested such a starch-regulating process. In T2 L appeared to be too high during the last 3 d, because starch was net depleted in the leaves. Hence, if the loading rate does not immediately adjust to substantial changes in assimilation rate due to changes in meteorological conditions (as was the case in the field, Fig. 2H), starch from the leaves is used and might act as a temporary buffer. In the roots, a continuous increase in starch was simulated, since the roots were the only sinks in the model.

Figures 3C, G and 4B, F show that during the night water was flowing in the plant although no transpiration occurred (Fig. 2C, G). This water flow which is circulating even when transpiration is zero is the so-called Münch's counterflow (Peuke *et al.*, 2001; Hölttä *et al.*, 2006). Münch's counterflow exists since loading and unloading processes continue during the night. It is commonly assumed that the contribution of Münch's counterflow to the total xylem flow is very low or negligible in transpiring leaves (Windt *et al.*, 2006). Simulations confirmed that during the day the phloem to xylem flow ratio was low (~5%) (Fig. 5). However, during the night, the ratio

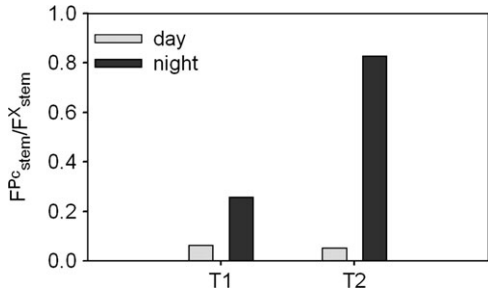

Fig. 5. The phloem to xylem ratio in the young oak tree (T1) and the adult beech tree (T2), indicating which part of the xylem flow is re-circulated by means of the phloem flow. Daytime ratios are shown in grey and night-time ratios in black.

increases to much higher values. This was also experimentally observed by Windt *et al.* (2006). Tanner and Beevers (2001) suggested that Münch's counterflow plays a significant role in the xylem circulation during the night and could be responsible for the distribution of minerals in the absence of transpiration or water uptake.

Conclusions

The mechanistic model describing coupled carbon and water fluxes showed realistic simulations when compared with real measured data obtained in both controlled and field conditions. The assigned parameter values correspondend to literature values. The model enabled simulation of several physiological variables (e.g. osmotic and turgor pressure in the phloem tubes, phloem sugar transport rates) which are often hard to measure experimentally. The model could confirm several reported literature observations: (i) the phloem transport is driven by a small pressure gradient and (ii) the phloem pressure changes in accordance with changes in transpiration. In addition, the model suggested daily dynamics in osmotic pressure which are experimentally confirmed in some instances, but not in others. The model was also able to simulate Münch's counterflow, which might be an important mechanism to redistribute minerals during the night. Increased knowledge on Münch's counterflow is also necessary to improve future sap flow calculation methods.

Supplementary data

Supplementary data are available at *JXB* online.

Figure S1. Schematic presentation of the initial assumptions leading to the initial set of equations.

Acknowledgements

We wish to thank the Research Foundation–Flanders (FWO) for the PhD funding granted to VDS and the Postdoctoral Fellow funding granted to KS. We are also indebted to Dr Dirk JW De Pauw (Phyto-IT) for his professional assistance with the sensitivity and identifiability analysis of the model, and to Philip Deman of the Laboratory of Plant Ecology for his accurate and enthusiastic technical support. Furthermore, we want to thank Maja Šimpraga and the Belgian Science Policy Office (BELSPO) (contract number SD/TE/03A) for funding the IMPECVOC research project which allowed us to obtain photosynthesis measurements on beech in the experimental forest of Ghent University.

References

Backes K, Leuschner C. 2000. Leaf water relations of competitive Fagus sylvatica and Quercus petraea trees during 4 years differing in soil drought. *Canadian Journal of Forest Research-Revue Canadienne de Recherche Forestiere* **30,** 335–346.

Borstlap AC, Schuurmans J. 2004. Sucrose transport into plasma membrane vesicles from tobacco leaves by H+ symport or counter exchange does not display a linear component. *Journal of Membrane Biology* **198,** 31–42.

Cosgrove D. 1986. Biophysical control of plant-cell growth. *Annual Review of Plant Physiology and Plant Molecular Biology* **37,** 377–405.

Cosgrove DJ. 2005. Growth of the plant cell wall. *Nature Reviews Molecular Cell Biology* **6,** 850–861.

Daudet FA, Ameglio T, Cochard H, Archilla O, Lacointe A. 2005. Experimental analysis of the role of water and carbon in tree stem diameter variations. *Journal of Experimental Botany* **56,** 135–144.

Daudet FA, Lacointe A, Gaudillére JP, Cruiziat P. 2002. Generalized Münch coupling between sugar and water fluxes for modelling carbon allocation as affected by water status. *Journal of Theoretical Biology* **214,** 481–498.

De Pauw DJW, Steppe K, De Baets B. 2008. Identifiability analysis and improvement of a tree water flow and storage model. *Mathematical Biosciences* **211,** 314–332.

Forsythe WE. 1954. 2003. *Smithsonian Physical Tables*. Knovel.

Frensch J, Hsiao TC. 1995. Rapid response of the yield threshold and turgor regulation during adjustment of root-growth to water-stress in Zea mays. *Plant Physiology* **108,** 303–312.

Gamalei YV. 2002. Assimilate transport and partitioning in plants: approaches, methods, and facets of research. *Russian Journal of Plant Physiology* **49,** 16–31.

Génard M, Fishman S, Vercambre G, Huguet J-G, Bussi C, Besset J, Habib R. 2001. A biophysical analysis of stem and root diameter variations in woody plants. *Plant Physiology* **126,** 188–202.

Goldhamer DA, Fereres E. 2004. Irrigation scheduling of almond trees with trunk diameter sensors. *Irrigation Science* **23,** 11–19.

Gould N, Minchin PEH, Thorpe MR. 2004. Direct measurements of sieve element hydrostatic pressure reveal strong regulation after pathway blockage. *Functional Plant Biology* **31,** 987–993.

Gould N, Thorpe MR, Koroleva O, Minchin PEH. 2005. Phloem hydrostatic pressure relates to solute loading rate: a direct test of the Munch hypothesis. *Functional Plant Biology* **32,** 1019–1026.

Granier A. 1985. A new method of sap flow measurement in tree stems. *Annales des sciences forestières* **42,** 193–200.

Granier A. 1987. Sap flow measurements in Douglas-Fir tree trunks by means of a new thermal method. *Annales des Sciences Forestières* **44,** 1–14.

Hammel HT. 1968. Measurement of turgor pressure and its gradient in phloem of oak. *Plant Physiology* **43,** 1042–1048.

Hölttä T, Vesala T, Sevanto S, Perämäki M, Nikinmaa E. 2006. Modeling xylem and phloem water flows in trees according to cohesion theory and Münch hypothesis. *Trees* **20,** 67–78.

Hsiao TC, Frensch J, Rojas-Lara BA. 1998. The pressure-jump technique shows maize leaf growth to be enhanced by increases in turgor only when water status is not too high. *Plant, Cell and Environment* **21,** 33–42.

Irvine J, Grace J. 1997. Continuous measurements of water tensions in the xylem of trees based on the elastic properties of wood. *Planta* **202,** 455–461.

Jones HG. 1992. *Plants and microclimate, a quantitative approach to environmental plant physiology*. Cambridge: Cambridge University Press.

Kedem O, Katchalsky A. 1958. Thermodynamic analysis of the permeability of biological membranes to non-electrolytes. *Biochimica et Biophysica Acta* **27,** 229–246.

Lacointe A, Minchin PEH. 2008. Modelling phloem and xylem transport within a complex architecture. *Functional Plant Biology* **35,** 772–780.

Le Roux X, Lacointe A, Escobar-Gutierrez A, Le Dizes S. 2001. Carbon-based models of individual tree growth: a critical appraisal. *Annals of Forest Science* **58,** 469–506.

Lee DR. 1981. Elasticity of phloem tissues. *Journal of Experimental Botany* **32,** 251–260.

Lockhart JA. 1965. An analysis of irreversible plant cell elongation. *Journal of Theoretical Biology* **8,** 264–275.

Münch E. 1930. *Die Stoffbewegunen in der Pflanze*. Jena: Gustav Fischer.

Murphy R, Ortega JKE. 1995. A new pressure probe method to determine the average volumetric elastic-modulus of cells in plant-tissue. *Plant Physiology* **107,** 995–1005.

Nelder JA, Mead R. 1965. A simplex-method for function minimization. *Computer Journal* **7,** 308–313.

Ortega JKE, Keanini RG, Manica KJ. 1988. Pressure probe technique to study transpiration in Phycomyces sporangiophores. *Plant Physiology* **87,** 11–14.

Peel AJ, Weatherley PE. 1962. Studies in sieve-tube exudation through aphid mouth-parts—effect of light and girdling. *Annals of Botany* **26,** 633–646.

Peramaki M, Nikinmaa E, Sevanto S, Ilvesniemi H, Siivola E, Hari P, Vesala T. 2001. Tree stem diameter variations and transpiration in Scots pine: an analysis using a dynamic sap flow model. *Tree Physiology* **21,** 889–897.

Perämäki M, Vesala T, Nikinmaa E. 2005. Modeling the dynamics of pressure propagation and diameter variation in tree sapwood. *Tree Physiology* **25,** 1091–1099.

Perez-Lopez D, Moriana A, Rapoport H, Olmedilla N, Ribas F. 2008. New approach for using trunk growth rate and endocarp development in the irrigation scheduling of young olive orchards. *Scientia Horticulturae* **115,** 244–251.

Peuke AD, Rokitta M, Zimmermann U, Schreiber L, Haase A. 2001. Simultaneous measurement of water flow velocity and solute transport in xylem and phloem of adult plants of Ricinus communis over a daily time course by nuclear magnetic resonance spectrometry. *Plant, Cell and Environment* **24,** 491–503.

Peuke AD, Windt C, Van As H. 2006. Effects of cold-girdling on flows in the transport phloem in Ricinus communis: is mass flow inhibited? *Plant, Cell and Environment* **29,** 15–25.

Pritchard J. 2007. Solute transport in the phloem. In: Yeo AR, Flowers TJ, eds. *Plant solute transport*. Oxford, UK: Blackwell Publishing, 253–274.

Proseus TE, Ortega JKE, Boyer JS. 1999. Separating growth from elastic deformation during cell enlargement. *Plant Physiology* **119,** 775–784.

Roberts J, Rosier PTW. 1994. Comparative estimates of transpiration of ash and beech forest at a Chalk site in Southern Britain. *Journal of Hydrology* **162,** 229–245.

Salleo S, Raimondo F, Trifilo P, Nardini A. 2003. Axial-to-radial water permeability of leaf major veins: a possible determinant of the impact of vein embolism on leaf hydraulics? *Plant, Cell and Environment* **26,** 1749–1758.

Sevanto S, Vesala T, Peramaki M, Nikinmaa E. 2003. Sugar transport together with environmental conditions controls time lags between xylem and stem diameter changes. *Plant, Cell and Environment* **26,** 1257–1265.

Sovonick-Dunford S, Lee DR, Zimmermann MH. 1981. Direct and indirect measurements of phloem turgor pressure in White Ash. *Plant Physiology* **68,** 121–126.

Steinberg S, Vanbavel CHM, McFarland MJ. 1989. A gauge to measure mass-flow rate of sap in stems and trunks of woody-plants. *Journal of the American Society for Horticultural Science* **114,** 466–472.

Steppe K, De Pauw DJW, Lemeur R. 2008. A step towards new irrigation scheduling strategies using plant-based measurements and mathematical modelling. *Irrigation Science* **26,** 505–517.

Steppe K, De Pauw DJW, Lemeur R, Vanrolleghem PA. 2006*a*. A mathematical model linking tree sap flow dynamics to daily stem diameter fluctuations and radial stem growth. *Tree Physiology* **26,** 257–273.

Steppe K, Lemeur R. 2004. An experimental system for analysis of the dynamic sap-flow characteristics in young trees: results of a beech tree. *Functional Plant Biology* **31,** 83–92.

Steppe K, Lemeur R, Dierick D. 2005. Unravelling the relationship between stem temperature and air temperature to correct for errors in sap-flow calculations using stem heat balance sensors. *Functional Plant Biology* **32,** 599–609.

Steppe K, Saveyn A, Vermeulen K, Lemeur R. 2006*b*. A comprehensive model for simulating stem diameter fluctuations and radial stem growth. In: *Proceedings of the IIIrd International Symposium on Models for Plant Growth, Environmental Control and*

Farm Management in Protected Cultivation. Leuven Belgium: International Society for Horticultural Science, 35–42.

Tanner W, Beevers H. 2001. Transpiration, a prerequisite for long-distance transport of minerals in plants? *Proceedings of the National Academy of Sciences, USA* **98,** 9443–9447.

Teskey RO, Saveyn A, Steppe K, McGuire MA. 2008. Origin, fate and significance of CO_2 in tree stems. *New Phytologist* **177,** 17–32.

Thomas SC, Malczewski G. 2007. Wood carbon content of tree species in Eastern China: interspecific variability and the importance of the volatile fraction. *Journal of Environmental Management* **85,** 659–662.

Thompson MV. 2006. Phloem: the long and the short of it. *Trends in Plant Science* **11,** 26–32.

Thompson MV, Holbrook NM. 2003. Scaling phloem transport: water potential equilibrium and osmoregulatory flow. *Plant, Cell and Environment* **26,** 1561–1577.

Tyree MT. 1988. A dynamic-model for water-flow in a single tree—evidence that models must account for hydraulic architecture. *Tree Physiology* **4,** 195–217.

Van Bel AJE. 2003. The phloem, a miracle of ingenuity. *Plant, Cell and Environment* **26,** 125–149.

van den Honert TH. 1948. Water transport in plants as a catenary process. *Discussion of the Faraday Society* **3,** 146–153.

Windt CW, Vergeldt FJ, De Jager PA, Van As H. 2006. MRI of long-distance water transport: a comparison of the phloem and xylem flow characteristics and dynamics in poplar, castor bean, tomato and tobacco. *Plant, Cell and Environment* **29,** 1715–1729.

Zweifel R, Item H, Hasler R. 2001. Link between diurnal stem radius changes and tree water relations. *Tree Physiology* **21,** 869–877.

Zweifel R, Zimmermann L, Zeugin F, Newbery DM. 2006. Intra-annual radial growth and water relations of trees: implications towards a growth mechanism. *Journal of Experimental Botany* **57,** 1445–1459.